SOLUTION COMBUSTION SYNTHESIS AND CHARACTERISTICS OF NANOSCALE MgO POWDERS

JIAHAI BAI, FANTAO MENG, CHUNCHENG WEI, YUNXIA ZHAO, HUIHUI TAN, JUNCHENG LIU

School of Materials Science and Engineering,
Shandong University of Technology, ZiBo, 255049, P. R. China

E-mail: zbbjh@sdut.edu.cn

Submitted November 3, 2010; accepted March 27, 2011

Keywords: MgO, Solution combustion synthesis, Nanocrystalline, Specific surface area

Nanoscale MgO powders were fabricated via a microwave-induced solution combustion process using $Mg(NO_3)_2$ and starch as starting materials. Effects of the relative fuel-to-oxidant ratios (φ_e = 1.1, 1.0, 0.9 and 0.8, respectively) on characteristics of MgO nanoparticles were also investigated. The XRD analysis discloses that MgO nanocrystalline are successfully synthesized and the crystalline size of MgO increases remarkably with increasing of φe from 0.8 to 1.1. TEM images reveal that nanoporous agglomerates of MgO nanocrystalline are formed in the powders. Experimental results show that the average particles' size of the powders decreases significantly as φe increases from 0.8 to 1.1. However, the powders from the precursors with φ_e equal to 1.0 exhibit larger specific surface area as compared the other powders.

INTRODUCTION

Nanoscale MgO powders have attracted great attention owing to its applications in many industrials areas, such as a candidate material for translucent ceramics [1], catalyst, catalyst carriers and absorbent for many pollutants [2]. Thus, many extensive studies have been carried out to synthesize nanoscale MgO powders using various novel wet chemical methods, e.g. sol-gel synthesis, followed by supercritical drying [3] and spray pyrolysis [4]. However, these techniques usually include many sophisticated processes and consume much longer time. Moreover, they have not received much commercial attention due to lacking of reproducibility, reliability and cost effectiveness [5, 6, 7]. At the same time, solution combustion synthesis may provide an answer to some of the above-mentioned problems. Therefore, extensive studies have been conducted to investigate solution combustion synthesis and characteristics of MgO powders. For example, the group of F. Granados-Correa synthesized MgO powders via a solution combustion process using urea as fuel [8]. In addition, K. V. Rao and C. S. Sunandana also fabricated MgO nanoparticles using the solution combustion technique with urea as fuel [9]. Moreover, Y. Mortazavi *et al* produced high activity MgO nanoparticles with large surface areas via a microwave-induced combustion process using polyethylene glycol and sorbitol as fuel [10]. In this work, MgO nanoparticles were synthesized via a microwave-induced combustion process using starch as fuel. In addition, effects of fuel to oxidant mole ratio on specific surface area, crystalline size and agglomerates' size distribution of the as-prepared powders were also investigated.

EXPERIMENTAL

Combustion synthesis

MgO powders were combustion synthesized using analytical purity $Mg(NO_3)_2{\cdot}6H_2O$ as oxidizer and soluble starch ($(C_6H_{10}O_5)_n$) as fuel. Since fuel-to-oxidant ratio in an oxidant-fuel mixture has a significant effect on combustion synthesis and characteristics of metal oxide nanoparticles, the relative fuel-to-oxidant ratio (φ_e) is calculated using the following formula:

$$\varphi_e = \frac{n\{6 \cdot 4_c + 10 \cdot 1_H + 5 \cdot (-2)_o\}}{-a\{1 \cdot 2_{Mg} + 2(1 \cdot O_N + 3 \cdot (-2)_o\}} \qquad (1)$$

where *n* is the mole fraction of the monomer of starch and *a* is the mole fraction of magnesium nitrate. A redox mixture is considered to be stoichiometric when $\varphi_e = 1$, fuel lean when $\varphi_e > 1$ and fuel rich $\varphi_e < 1$ [11]. Moreover, theoretically, a stoichiometric redox mixture could produce maximum energy during combustion [11]. In this work, MgO nanoparticles was fabricated using various redox mixtures with the starch monomer to magnesium nitrate mole ratio of 5.5: 12, 5: 12, 4.5: 12 and 4: 12,

respectively, i.e. φ_e is 1.1, 1.0, 0.9 and 0.8, respectively. Thereinafter, the four powders were named as powder A, B, C and D, respectively.

The typical experimental procedure is as follows: First, $Mg(NO_3)_2{\cdot}6H_2O$ was dissolved into 10 ml deionized water. Then the solution was heated up to 70 ˚C and kept for 30 min under magnetic stirring, followed by adding a certain amount of soluble starch into it. In all cases, 0.5 g of MgO was designed to be produced. After further magnetically stirred at 60°C till viscous gels were formed, the redox mixture contained in a china crucible was put into a domestic microwave oven, followed by being heated up with its maximum power (800 w). After several minutes, the solution precursors boiled, swelled, evolved a large amount of gases and finally ignited, followed by yielding products which was dissipated into fine agglomerates. Finally, the products were crushed in a mortar.

Thermodynamic modeling

To compare exothermicity of the various redox mixtures during combustion reactions, enthalpies of combustion and adiabatic flame temperature as a function of the fuel compositions were calculated.

Based on the propellant chemistry [12], combustion reactions in the four cases could be expressed as follows:

(A) φ_e = 1.1, fuel rich:

$$12\ Mg(NO_3)_2 \times 6\ H_2O + 5.5\ C_6H_{10}O_5 + 3\ O_2 \rightarrow \rightarrow 12\ MgO(s) + 12\ N_2(g) + 33\ CO_2(g) + 99.5\ H_2O(g) \quad (2)$$

(B) φ_e = 1.0, stoichiometric:

$$12\ [Mg(NO_3)_2 \times 6\ H_2O] + 5\ C_6H_{10}O_5 \rightarrow \rightarrow 12\ MgO(s) + 12\ N_2(g) + 30\ CO_2(g) + 97\ H_2O(g) \quad (3)$$

(C) φ_e = 0.9, fuel lean:

$$12\ [Mg(NO_3)_2 \times 6\ H_2O] + 4.5\ C_6H_{10}O_5 \rightarrow 12\ MgO(s) + + 12\ N_2(g) + 27\ CO_2(g) + 94.5\ H_2O(g) + 3\ O_2(g) \quad (4)$$

(D) φ_e = 0.8, fuel lean:

$$12\ [Mg(NO_3)_2 \times 6\ H_2O] + 4\ C_6H_{10}O_5 \rightarrow 12\ MgO(s) + + 12\ N_2(g) + 24\ CO_2(g) + 92\ H_2O(g) + 6\ O_2(g) \quad (5)$$

According to the thermodynamic data for the reactants and the products listed in Table 1, the enthalpies of combustion reactions and the theoretical adiabatic flame temperature as a function of the fuel-to-oxidant ratio were approximately calculated by the following equation [11]:

$$\Delta H = \sum n\Delta H_p - \sum n\Delta H_r = -\int_{T_0}^{Ta}(\sum nC_p)dT = -\int_{298}^{Ta}(\sum nC_p)dT \quad (6)$$

where ΔH_p and ΔH_r are the enthalpies of formation of the products and reactants, respectively, T_a is the theoretical adiabatic flame temperature, T_0 is the room temperature of 298 K; C_p is the molar heat capacity of products at constant pressure.

It is worth noting that C_p is a function of temperature and, generally, it is usually expressed as $C_p = A + BT + CT^2 + DT^3$ (A, B, C and D are constants). However, the peak adiabatic flame temperature reached during combustion is usually not too higher, so (CT^2 + DT^3) has little influence on the calculated adiabatic flame temperature. On the other hand, the calculated adiabatic flame temperature is theoretically and roughly determined using the thermodynamic data and it is not in good agreement with the actual flame temperature. Thus, C_p is nearly expressed as $C_p \approx A + BT$, as listed in Table 1, and used to calculate the adiabatic flame temperature.

Table 1. Relevant thermodynamics data.

Compound	ΔH_f (293 K) (Kcal mol^{-1})	C_p (cal (mol K)$^{-1}$)[a]
$Mg(NO_3)_2{\cdot}6\ H_2O$(c)	-622.21	–
$(C_6H_{10}O_5)_n$(c)	-401.57	–
MgO(c)	-143.23	11.2954 + 0.001358T
CO_2(g)	-94.05	10.34 + 0.00274T
H_2O(g)	-57.80	7.20 + 0.0036T
N_2(g)	0	6.5 + 0.0010T
O_2(g)	0	5.92 + 0.00367T

(c): crystalline; (g): gas; T: absolute temperature

[a] Calculated from the discrete values

Characterization

The phase compositions of the four products were determined using an X-ray diffractometer (XRD, D8 Advance, Brucker, Germany), equipped with a Ni-filtered Cu Kα radiation source (λ = 0.154178 nm). The average crystalline size was calculated according to XRD patterns using the peak corresponding to (200) plane and Scherrer formula as follows:

$$D_{XRD} = \frac{0.9\ \lambda}{\mathrm{FWHH} \cdot \cos\theta} \quad (7)$$

where D_{XRD} is the crystalline size (nm); λ is the radiation wavelength (0.154178 nm); FWHH is the full-width at half-maxima (radian); θ is the Bragg angle (degree).

The specific surface area of the powders was determined by BET (Brunauer-Emment-Teller) measurement (BELmax 00035, Ankersmid, Netherlands) on N_2 adsorption at 77 K after heat treatment at 523 K for 2 h. The grain equivalent diameter was calculated according to the specific surface using the following equation:

$$D_{BET} = \frac{6000}{\rho \cdot S} \quad (8)$$

where D_{BET} is the grain equivalent diameter (nm), ρ is the theoretical density of MgO (3.58 g·cm^{-3}) and S is the specific surface area (m^2·g^{-1}).

Microstructures of the as-prepared powders were characterized by transmission electron microscopy (TEM, H-800, HITACHI, Japan). The ignition losses (IOL) of the powders were determined by annealing them at 400 °C for 2 h .The particle size distribution analysis was conducted using a laser particle size analyzer (BN-2009, Bona Ltd, China).

RESULTS AND DISCUSSION

Enthalpies and adiabatic flame temperature of combustion

To investigate evolution of energy and flame temperature reached during combustion, the theoretical enthalpies of combustion and the theoretical adiabatic flame temperatures calculated according to the equation (6) as functions of the fuel-to-oxidant ratio are presented in Figure 1 and Figure 2, respectively.

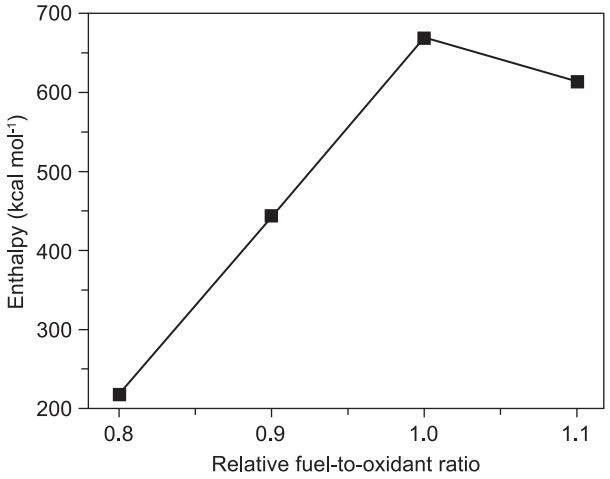

Figure 1. The calculated enthalpies of various combustion reactions as a function of the relative fuel-to-oxidant ratio.

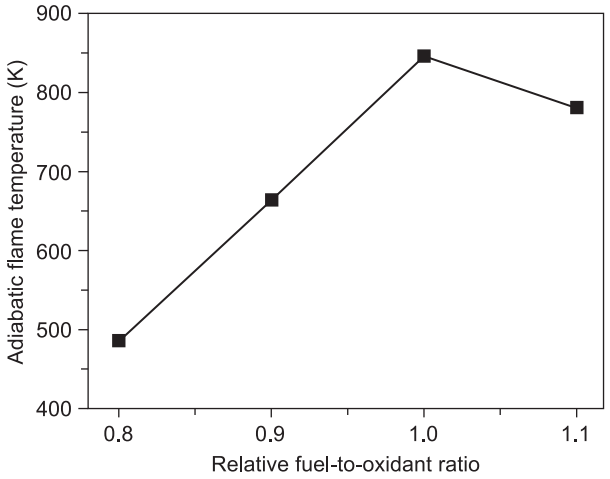

Figure 2. The theoretical adiabatic flame temperature reached during combustion as a function of the relative fuel-to-oxidant ratio.

As shown in Figures 1 and 2, the calculated enthalpies and the theoretical adiabatic flame temperature of the combustion reactions are significantly increased as the relative fuel-to-oxidant ratio rises from 0.8 to 1.0 and then remarkably fall when it is further climbs to 1.1. In other words, the stoichiometric mixture, theoretically, exhibits more energy and thus results in higher adiabatic flame temperature during combustion as compared with other mixtures.

XRD analysis

Figure 3 shows the XRD patterns of the four products synthesized using the microwave induced solution combustion process from the redox mixtures with φ_e equal to 1.1, 1.0, 0.9 and 0.8, respectively. As presented in Figure 3, the characteristic peaks of powders agree well with those of periclase (MgO, JCPDS 45-0946), revealing that the main crystal phase of the combustion synthesized powders is periclase. Moreover, the characteristic peaks of periclase become sharper and stronger as φ_e rises from 0.8 to 1.1, indicating that MgO crystalline are better crystallized and the naonocrystalline size which were calculated according to the Scherrer formula and listed in Table 2, is remarkably increased when the fuel-to-oxidant ratio (φ_e) increases. Since the four products were all subjected to heat treatment at 400 °C for 2 h, their difference in crystallization and crystalline size could be mainly attributed to flame temperature reached during combustion, i.e. flame temperature becomes higher as the relative fuel-to-oxidant ratio (φ_e) rises from 0.8 to 1.1. However, it is not in an agreement with the thermodynamic calculation presented in Figure 2, where the flame combustion temperature of the fuel lean (φ_e = 1.1) mixture is lower than that of the stoichiometric mixture (φ_e = 1.0). Since starch in neutral solutions begins to decompose at 90 □ [13], while $Mg(NO_3)_2$ decomposes remarkably at about 270°C, it is believed

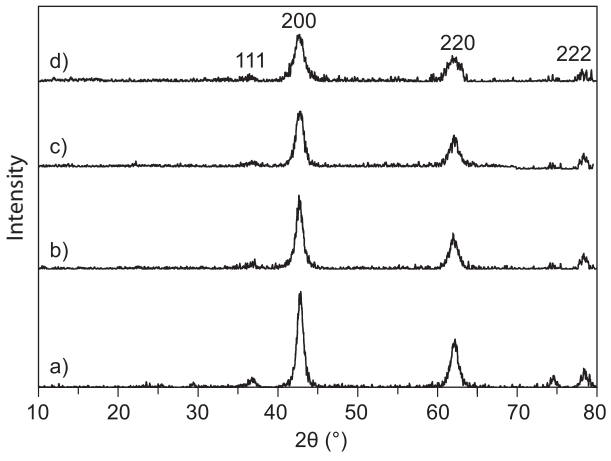

Figure 3. XRD patterns of the combustion synthesized products from the precursors with φ_e equal to a) 1.1, b) 1.0, c) 0.9 and d) 0.8, respectively.

that more starch may be decomposed (or oxidized) as compared to $Mg(NO_3)_2$ during the course of heating up under microwave irradiation. Therefore, the former would become closer to the stoichiometric composition, while the latter would become fuel lean. As a result, the actual flame temperature of the powder A would be higher than that of the powder B and could result in better crystallization, so sharper and narrower peaks occurs in the XRD patterns of the powder A.

Table 2. Characteristics of the combustion synthesized MgO powders.

Powder	φ_e	IOL (%)	XRD crystalline size DXRD (nm)	Specific surface area ($m^2\ g^{-1}$)	D_{BET} (nm)
A	1.1	40.3	8.3	58.6	28.6
B	1.0	40.0	7.6	60.5	27.7
C	0.9	35.3	6.6	45.6	35.2
D	0.8	29.5	5.5	39.5	42.4

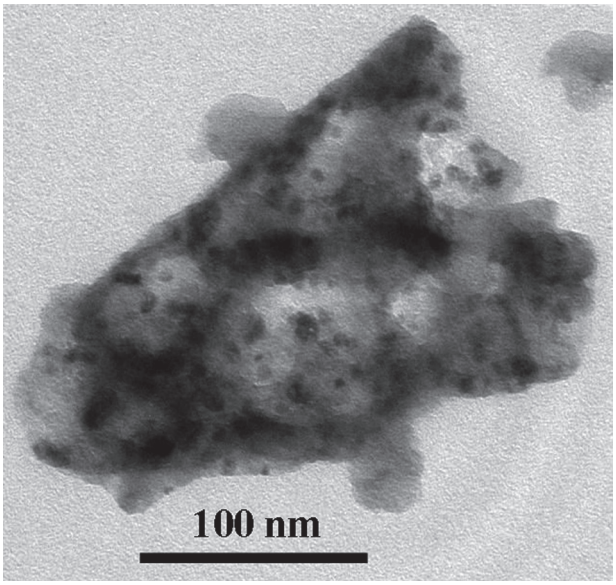

a)

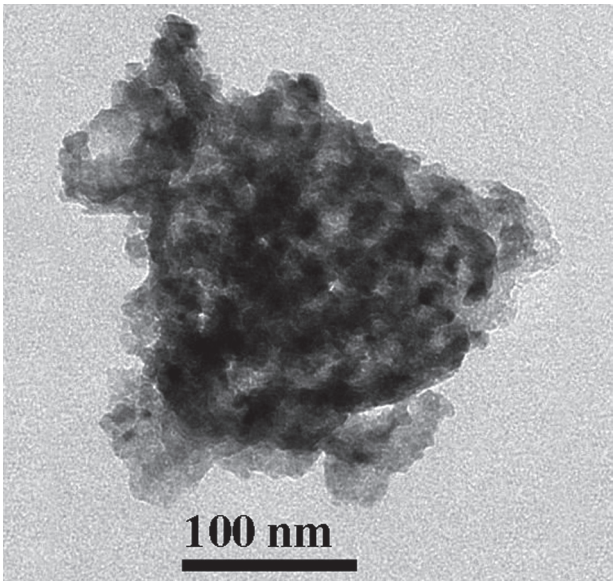

b)

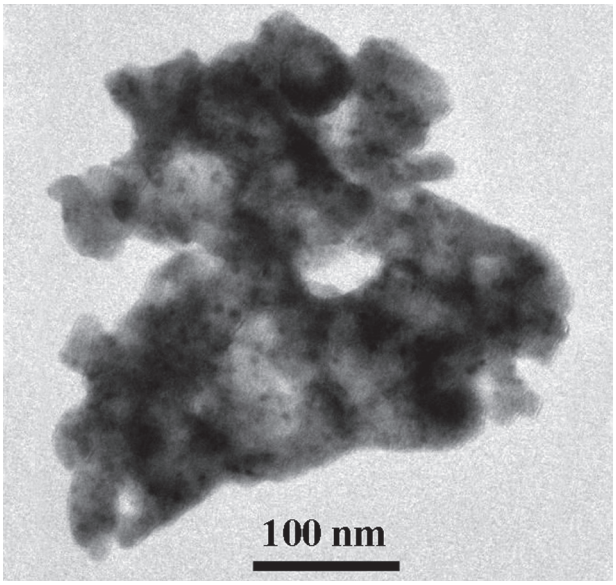

c)

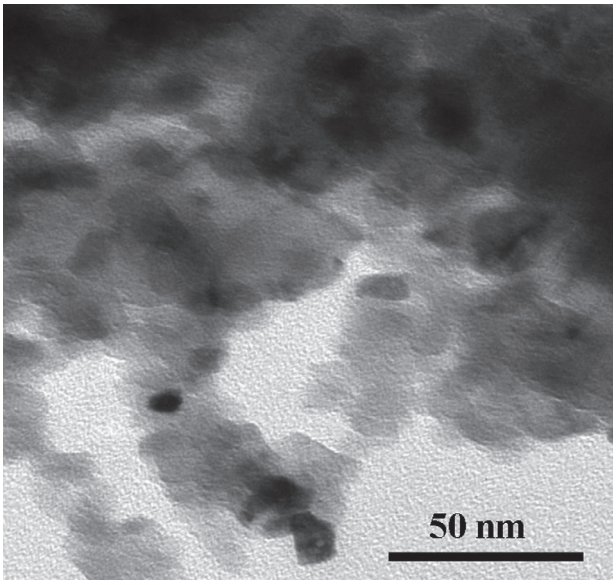

d)

Figure 4. TEM images of the MgO powders from the precursors with φ_e equal to a) 1.1; b, d) 1.0 and c) 0.9, respectively.

TEM microstructures

The TEM images of the three powders with φ_e = 1.1, 1.0 and 0.9, respectively, are presented in the Figure 4. As shown in Figure 4, hard agglomerates of MgO nano-crystalline in the three powders were all formed during combustion process. Furthermore, the agglomerates in the three powders are all nanoporous. Meanwhile, the porosity and the average size of the powder B appears to be larger than that of the powder A or C. However, it is hard to measure the average size of the MgO nano-crystalline due to hard agglomeration based on Figure 3abc. To determine the average size of the nano-crystalline, the further magnified image of the powder B is shown in Figure 3d. As can be seen, the average size of MgO nano-crystalline could be roughly determined to be no larger than 10 nm, in good agreement with the crystalline size calculated according to the XRD pattern and the Scherrer formula.

Particle (agglomerate) size distribution

To further clarify effects of the fuel-to-oxidant ratio on the characteristics of the combustion synthesized MgO powders, the particle (agglomerate) size distribution of the as-fabricated powders was measured and presented in Figure 5. As shown in Figure 5, the average particles' size is significantly decreased as the fuel-to-oxidant ratio (φ_e) increases from 0.8 to 1.1, especially when φ_e rises from 0.9 to 1.0, the medium size is sharply decreased from 7.01 μm to 2.08 μm, indicating that the fuel-to-oxidant ratio has a significant influence on particle size distribution of the combustion synthesized powders.

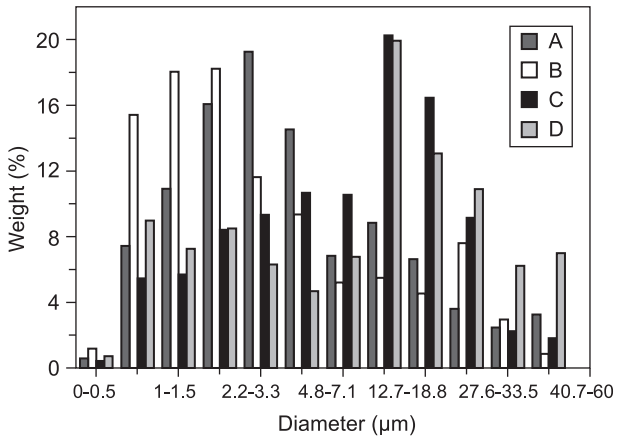

Figure 5. Particle size distribution of the combustion synthesized powders from the precursors with φ_e equal to A) 1.1, B) 1.0, C) 0.9 and D) 0.8, respectively.

Characteristics of the powders

The characteristics (IOL, XRD crystalline size, specific surface area) of the combustion synthesized MgO powders are listed in Table 2. As presented in Table 2, the IOL of the powders decreases slightly with decreasing of φ_e from 1.1 to 1.0, and then falls remarkably as φ_e decreases from 1.0 to 0.8. Meanwhile, the starch monomer to magnesium nitrate mole ratio in the precursors of the powder A, B, C and D is 5.5: 12, 5: 12, 4.5: 12 and 4:12, respectively, so the fuel to MgO weight ratio in the precursors could be roughly calculated as 1.87: 1, 1.69: 1, 1.51: 1 and 1.35: 1, respectively. Therefore, the fuel consumed during combustion process to MgO weight ratio of the powder A, B, C and D was 1.18:1, 1.02:1, 0.97:1 and 0.92:1, respectively, i.e. much more fuel was consumed during the combustion process of the powder A. So it can be inferred that higher flame temperature reached during combustion and thus MgO was better crystallized, agreeing well with the XRD analysis. Moreover, it also is concluded that the amount of gases evolved during combustion increases markedly as φ_e rises from 0.8 to 1.1, which was assumed to be mainly responsible for the significant increase in the average particles' size of the powders as φ_e climbs from 0.8 to 1.1 [14]. Furthermore, we observed that the combustion reaction of the redox precursors becomes more vigo-rous and the degree of dissipation of the particles becomes remarkably higher as φ_e rises from 0.8 to 1.1. Meanwhile, higher degree of dissipation may also make a contribution to decreasing the average particles' size. On the other hand, specific surface area of the powder B was slightly larger than that of the powder A, not in an agreement with the particles size distribution, which was mainly related to the nanoporous structures of the powders. As shown in Figure (4), there are much more nano-sized pores in the agglomerates of the powder A as compared with powder B, and the average nano-pore size of the former is larger than that of the latter. So the powder B exhibits slightly larger surface areas than the powder A, though the average particle size of the former is larger than that of the latter.

CONCLUSIONS

Nanoscale MgO powders were successfully fabricated via a solution combustion process using starch as fuel. Nanoporous agglomerates are formed in the powders. In addition, the XRD nanocrystalline size of the as-fabricated MgO powders is remarkably increased and the average particles' size of the powders is significantly decreased as φ_e rises from 0.8 to 1.1. However, the powder B (φ_e = 1.0) exhibits larger specific surface areas than the others powders.

References

1. Misawa T., Moriyoshi Y., Yajima Y., Takenouchi S., Ikegami T.: J. Ceram. Soc. Jpn. *107*, 343 (1999).
2. Chen L.M., Sun X.M., Liu Y.N., Li Y.D.: Appl. Catal. A: Gen. *265*, 123, (2004).
3. Bedilo A.F., Sigel M.J., Koper O.B., Melgunov M.S., Klabunde K.J.: J. Mater. Chem. *12*, 3599 (2002).
4. Seo D.J., Park S.B., Kang Y.C., and Choy K.L.: J. Nanopart. Res. *5*, 199 (2003).
5. Aruna S.T.: Curr. Opin. Solid. ST. M. Vol. 12, p. 40 (2008).
6. Patil K.C., Aruna S.T., Mimani T.: Curr. Opin. Solid. ST. M. Vol. 6, p. 507 (2002).
7. Ianos R., Lazau I.: Mater. Chem. Phys. *115*, 645 (2009).
8. Granados-Correa F., Bonifacio-Martínez J., Lara V.H., Bosch P., Bulbulian S.: Applied Surface Science *254*, 4688 (2008).
9. Venkateswara Rao K., Sunandana C.S.: J. Mater. Sci. *43*, 146 (2008).
10. Esmaeili E., Khodadadi A., Mortazavi Y.: Journal of the European Ceramic Society *29*, 1061 (2009).
11. Patil K.C., Hegde M.S., Tanu Rattan, Aruna S.T.: *Chemistry of nanocrystalline oxide materials: Combustion Synthesis, Properties and Applications*, p. 42-45, World Scientific, Singapore 2008.
12. Jain S.R., Adiga K.C., Pai Verneker V.R.: Combust. Flame. *40*, 71 (1981).
13. Veelaert S., de Wit D., Gotlieb K.F., Verhe R.: Carbohydrate Polymers *33*, 153 (1997).
14. Ganesh I., Srinivas B., Johnson R., Saha B.P., Mahajan Y.R.: Br. Ceram. Trans. *101*, 247 (2002).